Response of the Ionospheric TEC at the American low latitudes to SSW and storm-time induced SSW

[1]Fashae J.B., [1,2,3]Bolaji O.S. and [1,4]Rabiu A. B.

[1]Department of Physics and Solar Energy, Bowen University, Iwo, Nigeria

[2]Department of Physics, University of Lagos, Lagos, Nigeria

[3]Department of Mathematics and Physics, University of Tasmania, Hobart, Australia

[4] Center for Atmospheric Research, National Space Research & Development Agency, Anyigba, Nigeria

Abstract

We investigated the American low-latitude ionosphere around 75°W during the two 2013 sudden stratospheric warming (SSW) events: one in quiet geomagnetic conditions, and the other overlapped by a minor geomagnetic storm using total electron content (TEC) data from 12 Global Positioning System (GPS) receivers. A pair of magnetometers revealing the varying inferred vertical E X B drift and the NASA Thermosphere Ionosphere Mesosphere Energetics and Dynamics (TIMED) satellite airglow instrument to understand the global changes in the neutral composition, O/N_2 ratio are also used. The late morning inferred downward-directed E X B drift during the first major SSW did not support the varying equatorial ionization anomaly (EIA) signature. However, during the second major SSW, the well-reported and enhanced late morning inferred upward-directed E X B drift relocated a northern EIA crest to higher latitudes. Interestingly, the effect of minor geomagnetic storm on 17 January 2013 that modulated the ongoing second SSW reduced the maximum inferred upward-directed E X B drift. The second

major SSW contribution to the northern crest is higher than photo-ionization and the first major SSW contribution, while each major contribution is higher than minor warming. The minor geomagnetic storm reduced the effect of the second major SSW on the TEC from 58% to 50% and 28% to 20% at the northern and southern crest, respectively. Also, the storm's overall effect of - 1 % (22 %) leads to a slight reduction (enhancement) in TEC magnitude at the northern (southern) crest.

Keywords: low-latitude ionosphere, equatorial ionization anomaly (EIA), sudden stratospheric wind (SSW), geomagnetic storm.

Key points:

1. The late morning inferred download-directed E X B drift did not support the varying EIA signature during the first major SSW.
2. The late morning inferred upward-directed E X B drift relocated northern EIA crest to higher latitudes during the second major SSW.
3. The minor geomagnetic storm reduced the effect of the second major SSW on the ionospheric TEC at both crests.

1.0 Introduction

A daytime production of photo-ionization associated with solar extreme ultra-violet (EUV) radiation increases electron density at all the latitudes as discussed by Rishbeth et al. (2000) using solar radio flux as a proxy for solar EUV. In addition to photoionization during quiet geomagnetic conditions, the varying atmosphere neutral wind modulated electron density across all latitudes

(Balan et al., 2018). Compared to the high and middle latitudes, the equatorial and low-latitude ionosphere is also strongly associated with a transport process characterized by the equatorial electrojet (EEJ) strength, fountain effect and equatorial ionization anomaly (EIA). During the quiet conditions, the magnetic equator's daytime zonal electric field (EEJ strength) gets mapped into F-region through the magnetic field lines. This creates a vertical upward-directed $E\ X\ B$ drift that is responsible for removing plasma around the dip equator to higher altitudes as the new ionosphere develops at the lower altitudes (Balan et al., 1998). After losing momentum due to the force of gravity and electron density gradient, the uplifted plasma diffuses along the magnetic field lines to higher altitude on both sides of dip equator; a process called fountain effect (Hanson and Mofett, 1966; Balan and Bailey, 1995; Balan et al., 1997). This transport process led to a crest being formed on both sides of the low latitude and reduced the ionosphere plasma around the magnetic equator. This combined signature is referred to as equatorial ionization anomaly (EIA).

The magnetosphere-ionosphere coupling during a geomagnetic storm is a space weather event, which is generally referred to as forcing from above the ionosphere. During the magnetosphere-ionosphere coupling, almost all the atmosphere latitudes are modulated (Fuller-Rowell et al., 1994; Richmond and Lu, 2000). This is attributed to different large-scale physical processes like changes in the storm-time neutral atmospheric composition, the prompt penetration of electric field (PPEF), the ionospheric disturbance dynamo electric field (DDEF), solar heating, and thermospheric winds (Nishida, 1968; Vasyliunas, 1970, 1972; Gonzales et al., 1979; Blanc and Richmond, 1980; Fuller-Rowell et al., 1994, 1996). It is important to note that the varying storm-time equatorward wind and PPEF in the low latitudes that enhanced the EIA features (Tsurutani et al., 2008) and modulated it to an equatorial peak (Bolaji et al., 2021) can cause a more complex variability of the equatorial and low-latitude electrodynamics (Venkatesh et al., 2017).

It is also important to note that, aside from the famous space weather event that is due to a geomagnetic storm, studies have shown that a significant portion of day-to-day ionosphere variability is also related to forcing from the lower atmosphere, sudden stratospheric warming (SSW) event that coupled the ionosphere (Forbes et al., 2000; Lastovicka, 2006; Goncharenko et al., 2010a, b; Liu et al., 2013). SSW event is a meteorological phenomenon related to a rapid increase of the polar stratosphere temperature for several days during the northern winter. During this period, the zonal mean zonal wind that propagates westward decelerates (minor warming) or reverses to eastward (major warming) and interact non-linearly with the planetary wave (PW), resulting in the upward propagating waves towards the mesosphere lower thermosphere (MLT) region (Matsuno, 1971, Meyer, 1999). Energy and momentum transfer due to SSW events modulate the vertical ions drift (Chau et al. 2009, 2012; Fejer et al. 2010, 2011, Anderson & Araujo-Pradere, 2010)), equatorial electrojet (Yamazaki et al., 2012; Bolaji et al., 2016), and total electron content, TEC in the ionosphere (Chau et al., 2010; Goncharenko et al., 2010a; Liu et al., 2011; 2012; Korenkov et al., 2012; Fagundes et al., 2015; De Jesus et al., 2017; Bolaji et al., 2017, 2019).

A better understanding of the ionosphere response to SSW events that have remained one of the ongoing frontrunners about space weather is the key aim of this study. For example, January 2013 SSW event (7 January – 20 January 2013) is a peculiar one because three (3) space weather events characterized it: a minor SSW, major SSW and an ongoing major SSW modulated by a moderate geomagnetic storm. Furthermore, a major SSW condition was fulfilled on 7 January 2013 (first major SSW) and 12-20 January 2013 (second major SSW). A minor warming condition was met on 10 January 2013. A minor geomagnetic storm modulated the ongoing second major SSW on 17 January 2013. Maute et al. (2015) had also recognized the first and second major warmings,

but their attention was more focused on the second major warming (15-20 January 2013) because it was modulated by a moderate storm on 17 January 2013. Except for Maute et al. (2015), Hagan et al. (2015), Pedatella (2016) and Pedatella and Liu (2018) that used numerical simulations to investigate the combined effects of geomagnetic and meteorological activities on the ionosphere, the majority of earlier studies, especially in January 2013 were reported discretely. For instance, Goncharenko et al. (2013) and Jonah et al. (2014) studied the ionospheric effect of the 2013 SSW events over American low-latitude region using the GPS-TEC data. They reported strong perturbations in the TEC value at the crests of EIA compared to the background value and attributed it to the anomalous variations in vertical ion drift. Ribeiro et al. (2019) also used GPS-TEC data over the American sector to investigate the response of equatorial and low-latitudes positive ionospheric phases due to moderate geomagnetic during high solar activity in January 2013. They revealed significant changes in the electrodynamics of the ionosphere during the storm's main and recovery phases and attributed them to the travelling ionospheric disturbance (TID).

Although, these investigations have enlarged our scope of understanding about the SSW effect on the ionosphere on one side and the minor geomagnetic storm effect on another side. Most significantly, the effort of Maute et al. (2015) is acknowledged as they used vertical drift observations and the National Center for Atmospheric Research (NCAR) thermosphere-ionosphere-mesosphere electrodynamics general circulation model (TIME-GCM) to investigate ongoing major SSW that was modulated by a moderate geomagnetic storm on 17 January 2013. On this day, they observed an enhancement in the daytime vertical drift compared to 22 January 2013 (a non-SSW day) and attributed it to 50% contribution, each from SSW and a moderate geomagnetic storm effect. On the SSW effect, the increase in the wind dynamo leading to

enhancement in the daytime vertical drift was attributed to the migrating solar and semidiurnal westward propagating tides. The moderate geomagnetic storm effect was attributed to an increase in daytime vertical drift due to prompt penetration electric field (PPEF).

Despite these efforts, it is still unclear to the space weather community how this vertical drift characterized by a combined effect of a major SSW and minor geomagnetic storm on 17 January 2013 modulated the equatorial ionization anomaly (EIA) signature from GPS TEC observations. We will compare the effect of the first, minor and second major SSWs on the EIA signatures and discuss the interplay of photo-ionization, SSW and geomagnetic storm forcing that could be responsible for such changes. In addition, this study will demonstrate to the space weather community and document the contributions of the inferred vertical drift, photo-ionization, SSW and the minor geomagnetic storm effects to the low latitude crests.

2.0 Data and Methodology

Table 1 shows the list of station names, their codes, geographic and geomagnetic coordinates of the TEC data employed over 12 low-latitude stations along the American longitudes (Figure 1). The GPS TEC data were retrieved from cddis.nasa.gov/archive/gnss/data/. More details on GPS TEC analysis have been given in the works of Goncharenko et al. (2010b) and Bolaji et al. (2012). Figure 2 shows the varying stratospheric temperature, zonal mean zonal wind, solar flux, Kp index, IMF Bz and SYM-H during the months of December 2012 - February 2013 in panels a, b, c, d, and e, respectively. The stratospheric temperature started increasing significantly on 4 January 2013 (210 K) and reached its peak (239.9 K) on 7 January 2013 (shown between vertical red and green lines, Figure 2 panel a). This corresponds to more than 25 K increase in the stratospheric temperature at 10hPa within a week from 1 January to 10 January 2013 (Maute et al. 2015).

Coincidentally, on this same day of stratospheric temperature peak, the varying zonal mean zonal wind at 60 °N and 10 hPa turned eastward (shown in Figure 2 panel b). These indicate an ongoing major sudden stratospheric warming, SSW (classifies as first major warming). The stratospheric temperature begins a downward progression that lasts for about 3 days after the peak as the zonal mean zonal wind was reversing westward, an indicator of looming minor SSW. A major SSW was repeated on 12-20 January 2013 with the zonal mean zonal wind reaching a maximum of -12 m/s on 18 January 2013 (classifies as second major warming). These January 2013 SSW events coincided with the varying F10.7 in the range of 110 sfu - 168 sfu. While the second major SSW was ongoing, a minor geomagnetic storm started with SYM-H = -58 nT on 17 January 2013 (indicated by blue dotted lines). The varying IMF Bz was southward directed reaching - 15 nT.

Figures 3, 4, and 5 also indicate the stratospheric, solar, and geomagnetic parameters during the 2011/2012 (when $F_{10.7}$ = 140 sfu), 2013/2014 ($F_{10.7}$ = 168.2 sfu), and 2012/2013 (when $F_{10.7}$ = 120 sfu) SSW events (indicated by vertical dashed brown, blue and black lines) respectively. These periods are regarded as quiet periods for individual solar flux values while other parameters are relaxing. The stratospheric parameters consisting of the zonal mean zonal wind (60°N) and stratospheric temperature (90°N) at 10 hPa (~32km altitude) were retrieved from the NOAA Physical Sciences Laboratory at https://psl.noaa.gov/. This is used to study the influence of meteorological forcing on different current systems in the ionosphere. Further details regarding the NCEP-NCAR reanalysis data can be found in Kalnay et al. (1996). While, the geomagnetic (SYM-H and Kp), and solar (F10.7, IMF Bz) conditions were also obtained from the NASA OMNIweb service, https://omniweb.gsfc.nasa.gov/, and the National Oceanic and Atmospheric Administration (NOAA) solar data service at https://www.ngdc.noaa.gov/stp/solar/solardataservices.html. The neutral composition,

thermospheric O/N_2 column density data is optically obtained from NASA Thermosphere Ionosphere Mesosphere Energetics and Dynamics satellite (TIMED/GUVI) Far Ultraviolet (FUV) airglow instruments at http://guvitimed.jhuapl.edu.

Figures 6, 7 and 8 depict the corresponding daily TEC variability due to solar flux effect, when $F_{10.7}$ = 140 sfu (Figure 3), $F_{10.7}$ = 168.2 sfu (Figure 4) and $F_{10.7}$ = 120 sfu (Figure 5), (1sfu = $10^{-22}Wm^{-2}Hz^{-1}$) respectively. These solar flux values correspond to the values of the ongoing first major (when $F_{10.7}$ = 140 sfu), minor (when $F_{10.7}$ = 168 sfu) and second major (when $F_{10.7}$ = 119.8 sfu) warming events (Figure 2, panel c). The corresponding TEC values due to solar flux effect on Figures 6, 7 and 8 are averaged and denoted by TECquiet ($TECquietave_{(F10.7)}$). $TECquietave_{(F10.7)}$ simply implies the solar flux effect contributions to the low-latitude varying TEC while other parameters are not active (quiet period). Hence, during the first major SSW (7 January 2013), we deduced the contributions of SSW ($TEC_{(SSW)}$) to the varying TEC by subtracting the $TECquietave_{(F10.7)}$ in January 2012 (Figure 6, when $F_{10.7}$ = 140 sfu) from the TEC variations during the first major warming induced by solar flux ($TEC_{(SSW+F10.7)}$, Figure 9a). A similar approach was used to estimate the minor (10 January 2013, Figure 7) and second major (15 and 16 January 2013, Figure 8) SSW contributions to the varying ionospheric TEC. The station by station line plots of these individual contributions during the first major, minor and second major SSW are shown in Figures 10, 11, and 12 respectively. On 17 January 2013 that included both the ongoing SSW, $F_{10.7}$, and a minor geomagnetic storm ($TEC_{(SSW+F10.7+STORM)}$), the contribution of the $F_{10.7}$ (regarded as TECquiet when $F_{10.7}$ = 120 sfu, Figure 8) was deducted leaving the contribution of SSW and a minor geomagnetic storm ($TEC_{(SSW+storm)}$). Thereafter, the contribution of a minor geomagnetic storm ($TEC_{(STORM)}$) to the ongoing SSW-induced TEC was deduced by subtracting the SSW

contribution ($TEC_{(SSW)}$) on 16 January 2013 (as shown in Figure. 12, panel d) from $TEC_{(SSW+storm)}$ on 17 January 2013 (Figure. 13, panel c). All of these are mathematically expressed as follow:

$$TEC_{(SSW)} = TEC_{(SSW+F10.7)} - TECquietave_{(F10.7)} \quad (1)$$

$$TEC_{(SSW+STORM)} = TEC_{(SSW+F10.7+STORM)} - TECquietave_{(F10.7)} \quad (2)$$

$$TEC_{(STORM)} = TEC_{(SSW+STORM)} - TEC_{(SSW\ on\ 16\ January\ 2013)} \quad (3)$$

Where $TECquietave_{(F10.7)}$, $TEC_{(SSW+F10.7+STORM)}$, $TEC_{(SSW+F10.7)}$, $TEC_{(SSW)}$, and $TEC_{(STORM)}$ represent the averaged solar flux effect during the quiet period, the combined varying TEC consist of the SSW, solar flux and storm effects, varying TEC during ongoing SSW events induced by solar flux, TEC contribution due to SSW effect and TEC contribution due to storm effect, respectively.

More so, percentage contribution of the storm and SSW is as follow:

$$\%\ TEC_{(SSW)} = \frac{TEC(SSW)}{TEC(SSW+STORM)} * 100 \quad (4)$$

$$\%\ TEC_{(STORM)} = TEC_{(SSW\ +\ STORM)} - \%\ TEC_{(SSW)} \quad (5)$$

Conclusively, the individual contribution effect of SSW, solar flux and geomagnetic storm during the major and minor warmings are shown in Table 2.

3. 0 Results and Discussion

Figure 9a-9b shows the day-to-day EIA variations of TEC in the American low latitude ionosphere around 75^{o}W from 1 to 20 January 2013. The EIA crests seen around 18:00 UT (13:00 LT) on most of the days are higher at the northern crest, LPUC (4.25^{o}N), than the southern crest, IACR (5.58^{o}S). Some exceptions are seen during the second major SSW on 12-20 January 2013, where a higher EIA crest at IACR (5.58^{o}S) compared to LPUC (4.25^{o}N) characterized 12-14 January 2013. Also distinct is the re-location of the northern crest from LPUC to ESMR (4.25^{o}N to

13.02°N) on 14 January 2013 and its further re-location to BOGT (4.25°N to 16.93°N) on 15-19 January 2013. These results were related to the varying amplitude of the daily EEJ strength in Figure 14a-14b (magnetometer-inferred EXB drift velocity, Anderson and Araujo-Pradere, 2010) and variations in the thermospheric O/N_2 column density ratio (Figure 15). Similar results have been presented in the works of Goncharenko et al. (2013) and Siddiqui et al. (2018).

On 7 January 2013 (first major SSW), a daytime counter electrojet (CEJ) depicting a semidiurnal signature (downward in the morning-afternoon and upward in the afternoon-evening period) was seen in Figure 14a. This contrasts the well-reported semidiurnal upward (late morning) and downward (afternoon) varying equatorial EXB drift velocity signature (Chau et al., 2009; Sridharan et al., 2009; Fejer et al., 2010; Anderson and Araujo-Pradere, 2010) that increased the low latitude TEC and affected the EIA crests (Kelley, 2009). Recall that a semidiurnal signature indicates SSW-time semidiurnal tide in the varying equatorial EXB drift velocity (Chau et al., 2009; Fejer et al., 2010). Due to 2-dimensional pictures, such as a morning CEJ (Figure 14a) that can be related to a morning westward electric field and indicating that the daytime eastward electric field is not active, could not be seen in the works of Goncharenko et al. (2013) and Siddiqui et al. (2018). Therefore, a poleward plasma flow, which the eastward electric field can trigger, is rule-out in this context. To the best of our understanding, simulation and experimental investigations during geomagnetic conditions (Balan et al., 2009; Bolaji et al. 2021) have shown that the daytime westward electric field inhibited EIA formation and supported the formation of an equatorial peak. Hence, on 7 January 2013, the combined effects of the varying solar flux (photo-ionization production), SSW-time neutral wind and SSW-time thermospheric neutral composition O/N_2 ratio can be responsible for the EIA formation and its enhancement at the northern (LPUC) compared to the southern (IACR) crest. To clarify this, a major SSW depicted by dramatic changes

in the stratospheric temperature (239.9 K, Figure 2 panel a) and zonal mean zonal wind (- 5.64 m/s, Figure 2 panel b) at high latitudes on 7 January 2013 triggers the upward propagating waves interacting non-linearly with PW and propagating vertically towards the mesosphere lower thermosphere (MLT) region (Meyer, 1999). This set up an upward and equatorward circulation in the MLT region (Liu and Roble, 2002). Due to the heating of the high latitude thermosphere by the stratospheric temperature, meridional circulation changes associated with the varying SSW modulated the zonal mean zonal wind and connected the MLT with the middle and low latitude ionosphere (Laskar et al., 2014). As the suspected SSW-time equatorward wind due to heating of the thermosphere coupled the ionosphere with insignificant hindrance from the poleward plasma flow (especially at the middle latitudes), the ionosphere can be raised to higher altitudes of low recombination rate. Obviously, during the SSW-induced day of 7 January 2013, around 75^{o}W, the chemical effect due to the down-welling O/N_2 ratio (Roble, 1982) characterized by richer atomic oxygen and poorer molecular nitrogen at the northern high-middle latitudes is slightly higher than that of 6 January 2013 (Figure 15). The SSW-induced equatorward wind can bring along this slightly-high down-welling O/N_2 ratio seen at the northern high-middle latitudes to the low latitude ionosphere on 7 January 2013. Then, the combined effects of the SSW-time equatorward wind, a slight increase in the SSW-time down-welling effect and daytime photo-ionization production can facilitate the well-developed EIA signature and enhance the northern crest more than the southern crest on 7 January 2013. Recall that SSW is a northern winter phenomenon where its effect is dominant. This was supported by our results in Table 2, revealing that the SSW effect is the reason for a higher northern crest. For example, solar flux contributed 84% to the northern crest and 85% to the southern crest. In comparison, the SSW effect (SSW-time equatorward wind

252 and down-welling effect) contributed 16% and 15% to the northern and southern crest,
253 respectively.

254 A westerly-directed zonal mean zonal wind flow of 1m/s (Figure 2 panel b) observed on 10 January
255 2013 (a minor SSW) signifies a weak SSW-induced period which can be related to a weak SSW-
256 time equatorward wind varying in the thermosphere. In addition to this, is a weak (26 nT)
257 magnetometer-inferred upward EXB drift velocity (Figure 14a) seen around 75^{o}W depicting a
258 weak SSW-time eastward electric field in the ionosphere. Also, the SSW-time neutral composition
259 O/N_2 ratio on 10 January 2013 in American low latitude is weak (0.45). An exception is a
260 significant increase in solar flux from 140 sfu (7 January 2013) to 168 sfu (10 January 2013). This
261 was evident in Table 2 on 10 January 2013 as solar flux and SSW effects contributed 90% and
262 10%, respectively, to the northern crest. Solar flux contributed 77% at the southern crest and SSW
263 contributed 23%. These indicate that a minor SSW effect on the ionosphere is not remarkable in
264 the northern winter hemisphere on 10 January 2013. Therefore, combined effects of the above
265 physical mechanisms can be responsible for the EIA formation with photo-ionization production
266 as the leading factor.

267 Compared to 7 January 2013 first major SSW, significant re-location of the northern crest from
268 ESMR (14 January 2021) to BOGT station and its TEC enhancement on 15 and 16 January 2013
269 (second major SSW, Figure 9b) are attributed to intensified SSW conditions (stratospheric
270 temperature, T = 240 K, Figure 2 panel a and zonal mean zonal wind, U = - 5.72 m/s - -6.83 m/s,
271 Figure 2 panel b). These intensified SSW conditions modulate the varying semidiurnal inferred
272 EXB drift velocity on 14 January 2013 and significantly increase its value in the morning and CEJ
273 in the afternoon on 15-16 January 2013 (Figure 14b). As mentioned, a similar semidiurnal
274 signature in the inferred EXB drift velocity (Chau et al., 2009; Sridharan et al., 2009; Fejer et al.,

2010) increased the low latitude TEC and EIA crests (Kelley, 2009). This indicates a large increase in the daytime eastward electric field that transports more ionosphere plasma from around the magnetic equator through the magnetic field lines to higher altitudes. After losing momentum, due to gravity and electron density gradient, this large poleward ionosphere plasma flowing on both sides of the dip equator get deposited at higher latitudes.

In addition to this is the increase of thermospheric neutral composition O/N_2 ratio (Fig. 14) from 0.5 (14 January 2013) to 0.7 (15-16 January 2013). As the SSW-time equatorward wind was transporting the down-welling O/N_2 ratio into the low latitudes, it could not reduce the ongoing stronger poleward plasma flow in the northern hemisphere. Hence, the relocation of the northern crest from ESMR to BOGT while the southern crest location is not changing (Figure 9b). We suspect that the disparity in the hemispheric crests is related to the difference in the inferred EXB drift velocity between the northern and southern hemispheres. In addition to the well-reported thermospheric wind that modulated EIA crests, this is a future investigation as our inferred EXB drift velocity displayed in Figure 14b only originated from the northern hemisphere. The combined effect of SSW-time equatorward wind, indirect down-welling O/N_2 and stronger eastward electric field in the northern hemisphere contributed 58% (Table 2) to increase in TEC magnitude at the northern crest and its relocation. Together with the ongoing daytime production of ionization that contributed 42%, they are responsible for these significant changes seen in EIA signatures on 15-16 January 2013. However, in the southern hemisphere, where the SSW effect rarely modulates the ionosphere, photo-ionization contribution was more prominent (72%) than SSW, which contributed 28%.

On 17 January 2013, our results (Figure 9b, Figure 14b and day 17 in Figure 15) revealed that the effect of the ongoing intense SSW got modulated by a minor geomagnetic storm (SYM-H of - 58

nT), storm-time induced SSW. Contrasting Pedatella et al. (2008)'s work, the ongoing major SSW altered by a minor geomagnetic storm on 17 January 2013 did not disrupt the SSW-induced EIA signature but modulated it by reducing the northern crest and increasing the southern crest to ~ 75 TECU and ~ 77 TECU, respectively (Figure 9b). This reduction of SSW effect on the ionosphere by the minor geomagnetic storm of 17 January 2013 is interestingly evidenced in Figure 14b as the inferred upward-directed EXB maximum observed in the northern hemisphere was reduced compared to prior and after the SSW-induced days (15,16, 18 and 19 January 2013). Also, as shown in Table 2, the minor geomagnetic storm reduced SSW contributions at the northern crest to 50% and increased the photo-ionization contribution to 51%. Therefore, the overall reduction contributed by the minor geomagnetic storm to both effects was -1%. At the southern crest, the minor geomagnetic storm reduces both the photo-ionization (58%) and SSW (20%) effects compared to 15-16 January 2013 (Table 2). Then, the minor geomagnetic storm contributed 22% to both effects at the southern crest. Overall, the minor geomagnetic storm reduced (increased) the northern (southern) crest on 17 January 2013. Our results agree with the work of Ribeiro et al. (2019) on the higher southern crest of 17 January 2013 (77 TECU) compared to 16 January 2013 (65 TECU). However, their suggestion of invoking travelling ionospheric disturbances, TIDs cannot be substantiated as the varying TEC residual wave-form reported in their work is actually of SSW origin, as shown by our efforts in this work (Figure 13 panel e). Also, our results strongly disagree with the suggestion of Goncharenko et al. (2013) that a brief minor geomagnetic activity of 17 January 2013 will not drive these above-described variations in the low latitude TEC. Our observed results strongly agree with the suggestions of Maute et al. (2015), Hagan et al., 2015, Pedatella (2016) and Pedatella and Liu (2018) in that combined effect of the lower atmospheric

forcing and a geomagnetic storm is important to specifying and forecasting the near-Earth space environment.

4.0 Conclusions

In this paper, we have presented and discussed the response of the low latitude ionosphere in the American sector to the 2013 SSW event and a minor geomagnetic storm overlapping it on 17 January 2013. The main results from the study are as follow:

1. The late morning inferred downward-directed E X B drift was inactive in the formation of EIA signature during the first major warming. During the second major warming, the upward directed late morning-near inferred upward-directed E X B drift leads to the relocation of plasma to higher latitude during the second major warming.
2. With or without the inferred E X B drift, a well-developed EIA signature during SSW events is due to the combined effects of increase in SSW-time equatorward wind, SSW-time down-welling O/N_2 effect and daytime photo-ionization production.
3. The reduction of SSW effect on the ionosphere by the minor geomagnetic storm of 17 January 2013 correlated with reduced inferred upward-directed EXB drift maximum observed in the northern hemisphere compared to prior and after the SSW-induced days.
4. The SSW effect that contributed 16% (58%) to the northern crest during the first (second) major warmings is higher than 10% contributed to the northern crest during minor warming.
5. The storm-time induced SSW causes slight reduction and increment in the TEC magnitude at northern and southern crest, respectively.
6. The overall reduction contributed by the moderate geomagnetic storm to both SSW, and the photoionization effect was - 1% at the northern crest and 22% at the southern crest.

7. Contrary to the assertion of Pedatella et al. (2008) while studying event of July 2004, the interplay between the ongoing SSW and geomagnetic storm of 17 January 2013 did not disrupt the EIA signature but modulated it by reducing (increasing) the northern (southern) crest.
8. Our observation that agreed with the intensification of ionospheric plasma seen at the southern crest in the work of Ribeiro et al. (2019) contrasted their suggestions of being driven by TID of gravity waves origin. Actually, a major SSW was ongoing prior to being overlapped by a brief and minor geomagnetic storm.
9. Contrary to Goncharenko et al. (2013) suggestion, our observed results revealed that geomagnetic activity, among others, is a factor to reckon with in driving the ionospheric variations seen on 17 January 2013. Hence, modellers should start considering SSW forcing along geomagnetic storm forcing in their future modelling efforts. This would improve the forecasting of the near-Earth space environment.

Finally, we concluded that it is now becoming increasingly clear that understanding the forcing from SSW is critically important for the space weather modelling community to predict and forecast the day-to-day TEC during the northern wintertime in the low latitude. Thus, incorporating the forcing due to SSW during the northern wintertime into the future modelling efforts is critically important to accurately characterize the day-to-day variability of TEC in the low latitude ionosphere.

Acknowledgments

The stratospheric, geomagnetic and solar activity data used in this study were retrieved from the websites of the NOAA Physical Sciences Laboratory (https://psl.noaa.gov), NASA OMNIweb

service, https://omniweb.gsfc.nasa.gov/, and the National Oceanic and Atmospheric Administration (NOAA), solar data service at https://www.ngdc.noaa.gov/stp/solar/solardataservices.html respectively. The total electron content (TEC) data from the Global Positioning System (GPS) receivers are freely available online via National Aeronautics and Space Administration (NASA) Archive of Space Geodesy Data (cddis.nasa.gov/archive/gnss/data/) and SONEL (www.sonel.org). The magnetometer data were downloaded from the International Real-time Magnetic Observatory Network, INTERMAGNET (www.intermagnet.org), and the Low Ionospheric Sensor Network (LISN) magnetometers (http:// lisn.igp.gob.pe/data/) operated by the Instituto Geofisico del Peru (IGP). The thermospheric O/N_2 column density data is optically obtained from NASA Thermosphere Ionosphere Mesosphere Energetics and Dynamics satellite (TIMED/GUVI) Far Ultraviolet (FUV) airglow instruments at http://guvitimed.jhuapl.edu. The authors thank Gopi Seemala for providing the GPS TEC processing software.

References

Anderson, D., & Araujo-Pradere, E. A. (2010). Sudden stratospheric warming event signatures in daytime ExB drift velocities in the Peruvian and Philippine longitude sectors for January 2003 and 2004. Journal of Geophysical Research: Space Physics, 115(8), 1–7. https://doi.org/10.1029/2010JA015337

Balan, N., K. Shiokawa, Y. Otsuka, S. Watanabe, and G. J. Bailey (2009), Super plasma fountain and equatorial ionization anomaly during penetration electric field, J. Geophys. Res., 114, A03310, doi: 10.1029/2008JA013768.

388 Balan, N., Souza, J., & Bailey, G. J. (2018). Recent developments in the understanding of
389 equatorial ionization anomaly: A review. Journal of Atmospheric and Solar-Terrestrial
390 Physics, 171, 3–11. doi:10.1016/j.jastp.2017.06.020

391 Blanc, M., and A. D. Richmond (1980). The ionospheric disturbance dynamo, J. Geophys. Res.
392 85(A4), 1669– 1686.

393 Bolaji, O. S., J. O. Adeniyi, S. M. Radicella and P. H. Doherty (2012), Variability of total
394 electron content over an equatorial West African station during low solar activity, Radio
395 Science, 47, RS1001, doi:10.1029/2011RS004812.

396 Bolaji, O. S., Owolabi, O. P., Falayi, E., Jimoh, E., Kotoye, A., Odeyemi, O., et al. (2016). Solar
397 quiet current response in the African sector due to a 2009 sudden stratospheric warming
398 event. Journal of Geophysical Research: Space Physics, 121, 8055–8065. https://doi.
399 org/10.1002/2016JA022857

400 Bolaji, O., Owolabi, O., Falayi, E., Jimoh, E., Kotoye, A., Odeyemi, O., … Onanuga, K.
401 (2017). Observations of equatorial ionization anomaly over Africa and Middle East during a
402 year of deep minimum. Annales Geophysicae, 35(1), 123–132. doi:10.5194/angeo-35-123-
403 2017

404 Bolaji, O. S., Oyeyemi, E. O., Jimoh, O. E., Fujimoto, A., Doherty, P. H., Owolabi, O. P., et al
405 (2019). Morphology of the equatorial ionization anomaly in Africa and Middle East due to a
406 Sudden stratospheric warming event. Journal of Atmospheric and Solar-Terrestrial Physics,
407 184, 37–56. https://doi.org/10.1016/j.jastp.2019.01.006

408 Bolaji, O. S., Fashae, J. B., Adebiyi, S. J., Owolabi, C., Adebesin, B. O., Kaka, R. O. (2021). Storm
409 time effects on latitudinal distribution of ionospheric TEC in the American and Asian-

Australian sectors: August 25–26, 2018 geomagnetic storm. Journal of Geophysical Research: Space Physics, 126, e2020JA029068. https://doi.org/10.1029/2020JA029068.

Chau, J. L., Fejer, B. G., & Goncharenko, L. P. (2009). Quiet variability of equatorial e × B drifts during a sudden stratospheric warming event. *Geophysical Research Letters*, *36*(5), 1–4. https://doi.org/10.1029/2008GL036785

Chau, J. L., Aponte, N. A., Cabassa, E., Sulzer, M. P., Goncharenko, L. P., & Gonzlez, S. A. (2010). Quiet time ionospheric variability over Arecibo during sudden stratospheric warming events. *Journal of Geophysical Research: Space Physics*, *115*(9), 2–9. https://doi.org/10.1029/2010JA015378

Fagundes, P.R., Cardoso, F.A., Fejer, B.G., Venkatesh, K., Ribeiro, B.A. G., Pillat, V.G., 2016. Positive and negative GPS-TEC ionospheric storm effects during the extreme space weather event of March 2015 over the Brazilian sector. J. Geophys. Res.: Space Phys. 121 (6), 5613–5625. https://doi.org/10.1002/2015JA022214.

Fejer, B. G., Olson, M. E., Chau, J. L., Stolle, C., Ïhr, H., Goncharenko, L. P., Yumoto, K., & Nagatsuma, T. (2010). Lunar-dependent equatorial ionospheric electrodynamic effects during sudden stratospheric warmings. *Journal of Geophysical Research: Space Physics*, *115*(8), 1–9. https://doi.org/10.1029/2010JA015273

Fejer, B. G., Tracy, B. D., Olson, M. E., & Chau, J. L. (2011). Enhanced lunar semidiurnal equatorial vertical plasma drifts during sudden stratospheric warmings. *Geophysical Research Letters*, *38*(21), 2–6. https://doi.org/10.1029/2011GL049788

Forbes, J. M. (2000), Wave coupling between the lower and upper atmosphere: Case study of an ultra-fast Kelvin wave, J. Atmos. Sol. Terr. Phys., 62, 1603–1622.

Fuller-Rowell, T. J., Codrescu, M. V., Moffett, R. J., and Quegan, S. (1994), Response of the thermosphere and ionosphere to geomagnetic storms. *Journal of Geophysical Research*, *99*(A3), 3893. https://doi.org/10.1029/93JA02015

Fuller-Rowell, T. J., M. V. Codrescu, H. Rishbeth, R. J. Moffett, and S. Quegan (1996), On the seasonal response of the thermosphere and ionosphere to geomagnetic storms, J. Geophys. Res., 101, 2343–2353, doi:10.1029/95JA01614.

Goncharenko, L. P., J. L. Chau, H.-L. Liu, and A. J. Coster (2010a), Unexpected connections between stratosphere and ionosphere, Geophys.Res. Lett., 37, L10101, doi:10.1029/2010GRL043125.

Goncharenko, L. P., A. J. Coster, J. L. Chau, and C. E. Valladares (2010b), Impact of sudden stratospheric warming on equatorial ionization anomaly, J. Geophys. Res., 115, A00G07, doi:10.1029/2010JA015400.

Goncharenko, L., Chau, J. L., Condor, P., Coster, A., & Benkevitch, L. (2013). Ionospheric effects of sudden stratospheric warming during moderate-to-high solar activity: Case study of January 2013. *Geophysical Research Letters*, *40*(19), 4982–4986. https://doi.org/10.1002/grl.50980

Gonzales, C. A., M. C. Kelley, B. G. Fejer, J. F. Vickrey, and R. F. Woodman (1979), Equatorial electric fields during magnetically disturbed conditions: 2. Implications of simultaneous auroral and equatorial measurements, J. Geophys. Res., 84, 5803–5812, doi:10.1029/ JA084iA10p05803.

Hagan, M. E., K. Häusler, G. Lu, J. M. Forbes, and X. Zhang (2015), Upper thermospheric responses to forcing from above and below during 1–10 April 2010: Results from an ensemble of numerical simulations, J. Geophys. Res. Space Physics, 120, 3160–3174, doi: 10.1002/2014JA020706.

Kalnay, E., Kanamitsu, M., Kistler, R., Collins, W., Deaven, D., Gandin, L., et al. (1996). The NCEP/NCAR 40-year reanalysis project. Bulletin of the American Meteorological Society, 77(3), 437–471. https://doi.org/10.1175/1520-0477(1996)077<0437:TNYRP>2.0.CO;2.

Kelley, M. C, Ilma, R. R. and G. Crowley (2009), On the origin of pre-reversal enhancement of the zonal equatorial electric field Ann. Geophys., 27, 2053–2056, 2009 www.ann-geophys.net/27/2053/2009/

Laskar, F. I., Pallamraju, D., & Veenadhari, B. (2014). Vertical coupling of atmospheres: Dependence on strength of sudden stratospheric warming and solar activity. *Earth, Planets and Space*, *66*, 1–10. https://doi.org/10.1186/1880-5981-66-94

Laštovička, J. (2006), Forcing of the ionosphere by waves from below, J. Atmos. Sol. Terr. Phys., 68(3–5), 479–497, doi:10.1016/j.jastp.2005.01.018.

Liu, H.-L., & Roble, R. G. (2002). A study of a self-generated stratospheric sudden warming and its mesospheric-lower thermospheric impacts using the coupled TIME-GCM/CCM3. Journal of Geophysical Research: Atmospheres, 107(D23), ACL 15–1–ACL 15–18. doi:10.1029/2001jd001533

Liu, H., E. Doornbos, M. Yamamoto, and S. Tulasi Ram (2011), Strong thermospheric cooling during the 2009 major stratosphere warming, Geophys. Res. Lett., 38, L12102, doi:10.1029/2011GL047898.

Liu, H.-L., and A. D. Richmond (2013), Attribution of ionospheric vertical plasma drift perturbations to large-scale waves and the dependence on solar activity, J. Geophys. Res. Space Physics, 118, 2452–2465, doi:10.1002/jgra.50265.

Matsuno, T. (1971). A Dynamical Model of the Stratospheric Sudden Warming. Journal of the Atmospheric Sciences. https://doi.org/10.1175/1520-0469 (1971)028<1479.

Maute, A., Hagan, M. E., Yudin, V., Liu, H. L., & Yizengaw, E. (2015). Causes of the longitudinal differences in the equatorial vertical e × B drift during the 2013 SSW period as simulated by the TIME-GCM. Journal of Geophysical Research A: Space Physics. https://doi.org/10.1002/2015JA021126

Meyer Christian K. (1999). Gravity wave interactions with the diurnal propagating tide, Journal of Geophysical Research, vol. 104, no. D4, Pages 4223-4239, February 27, 1999

Nishida, A. (1968), Coherence of geomagnetic DP2 magnetic fluctuations with interplanetary magnetic variations, J. Geophys. Res., 73(17), 5549–5559.

Pedatella, N. M., J. M. Forbes, J. Lei, J. P. Thayer, and K. M. Larson (2008), Changes in the longitudinal structure of the low-latitude ionosphere during the July 2004 sequence of geomagnetic storms, J. Geophys. Res., 113, A11315, doi:10.1029/2008JA013539.

Pedatella, N. M., Fang, T.-W., Jin, H., Sassi, F., Schmidt, H., Chau, J. L., et al. (2016). Multimodel comparison of the ionosphere variability during the 2009 sudden stratosphere warming. Journal of Geophysical Research: Space Physics, 121, 7204–7225. https://doi.org/10.1002/2016JA022859.

Pedatella, N. M., & Liu, H.-L. (2018).The Influence of Internal Atmospheric Variability on the Ionosphere Response to a Geomagnetic Storm. Geophysical Research Letters, 45(10), 4578–4585. doi:10.1029/2018gl077867

Ribeiro, B. A. G., Fagundes, P. R., Venkatesh, K., Tardelli, A., Pillat, V. G., & Seemala, G. K. (2019). Equatorial and low-latitude positive ionospheric phases due to moderate geomagnetic storm during high solar activity in January 2013. *Advances in Space Research*, *64*(4), 995–1010. https://doi.org/10.1016/j.asr.2019.05.032

Richmond, A. D., and G. Lu (2000), Upper-atmospheric effects of magnetic storms: A brief tutorial, J. Atmos. Sol. Terr. Phys., 62, 1115–1127, doi:10.1016/S1364-6826(00)00094-8.

Rishbeth, H., Muller-Wodarg, I.C.F., Zou, L., Fuller-Rowell, T.J., Millward, G.H., Moffett, R.J., Idenden, D.W., Aylward, A.D., 2000. Annual and semiannual variations in the ionospheric F2-layer: II. Physical discussion. Ann. Geophys. 18, 945–956. https://doi.org/10.1007/s00585-000-0945-6.

Roble, R. G., R. E. Dickinson, and E. C. Ridley (1982), Global circulation and temperature structures of thermosphere with high-latitude plasma convection. *J. Geophys. Res*., 87, 1599–1614.

Sridharan, S., S. Sathishkumar, and S. Gurubaran (2009). Variabilities of mesospheric tides and equatorial electrojet strength during major stratospheric warming events, Ann. Geophys., 27, 4125–4130, 2009, www.ann-geophys.net/27/4125/2009/

Siddiqui Tarique A., Astrid Maute, Nick Pedatella, Yosuke Yamazaki, Hermann Lühr, and Claudia Stolle (2018). On the variability of the semidiurnal solar and lunar tides of the equatorial electrojet during sudden stratospheric warmings, Ann. Geophys., 36, 1545–1562, 2018 https://doi.org/10.5194/angeo-36-1545-2018.

Tsurutani, B.T., O.P. Verkhoglyadova, A.J. Mannucci, A. Saito, T. Araki, et al., Prompt penetration electric fields (PPEFs) and their ionospheric effects during the great magnetic storm of 30–32 October 2003, J. Geophys. Res., 113, A05311, DOI: 10.1029/2007JA012879, 2008b.

Vasyliunas, V. M. (1970). Mathematical models of magnetospheric convection and its coupling to the ionosphere. In M. McCormac (Ed.), *Particles and fields in the magnetosphere*, (pp. 60–71). New York: Springer.

Vasyliunas, V. M. (1972), The interrelationship of magnetospheric processes. In B. M. McCormac (Ed.), *Earth's magnetosphere processes*, (pp. 29–38). Norwell, Mass: D. Reidel.

527 Venkatesh, K., Ram, S.T., Fagundes, P.R., Seemala, G.K., Batista, I.S., 2017. Electrodynamic
528 disturbances in the Brazilian equatorial and lowlatitude ionosphere on St. Patrick's Day
529 storm of 17 March 2015. J. Geophys. Res.: Space Phys. 122 (4), 4553–4570. https://doi.org/
530 10.1002/2017JA024009.

	Station Location	Country	Station Codes	Geographical Coordinates	Geomagnetic Coordinates
1.	Magangue	Colombia	VMAG	9.29^0N, 74.85^0W	21.43^0N, 357.56^0W
2.	Bogota	Colombia	BOGT	4.71^0N, 74.07^0W	16.93^0N, 358.11^0W
3.	Esmeraldas	Ecuador	ESMR	0.96^0N, 79.65^0W	13.02^0N, 351.56^0W
4.	Puengasi	Ecuador	QUEM	0.24^0S, 78.49^0W	11.96^0N, 352.82^0W
5.	Pucallpa	Peru	LPUC	8.38^0S, 74.57^0W	4.25^0N, 356.88^0W
6.	Huancanyo	Peru	IHYO	12.04^0S, 75.32^0W	0.63^0N, 356.08^0W
7.	Galeras	Peru	GLRV	14.67^0S, 74.40^0W	1.89^0S, 357.01^0W
8.	Arica	Chile	IACR	18.47^0S, 70.33^0W	5.58^0S, 0.70^0W
9.	Antofagasta	Chile	VCNF	23.68^0S, 70.41^0W	10.58^0S, 0.58^0W
10.	Copiapo	Chile	COPO	27.38^0S, 70.33^0W	14.10^0N, 0.69^0W
11.	Valparaiso	Chile	VALN	33.02^0S, 71.63^0W	19.38^0S, 359.97^0W
12.	Talcahuano	Chile	CONZ	36.84^0S, 73.02^0W	22.96^0S, 359.34^0W

531 Wei, Y., Zhao, B., Guozhu, G., Wan, W., 2015. Electric field penetration into Earth's ionosphere:
532 a brief review for 2000–2013. Sci. Bull. 60 (8), 748–761. https://doi.org/10.1007/s11434-
533 015-0749-4.
534 Yamazaki, Y., Yumoto, K., McNamara, D., Hirooka, T., Uozumi, T., Kitamura, K., Abe, S., &
535 Ikeda, A. (2012). Ionospheric current system during sudden stratospheric warming events.
536 *Journal of Geophysical Research: Space Physics*, *117*(3), 1–7.
537 https://doi.org/10.1029/2011JA017453

538

539 Table 1: Details of Global Positioning Systems (GPS) Station Names, Station Codes, Geographic
540 and Geomagnetic Longitudes and Latitudes.

541

542

543

544

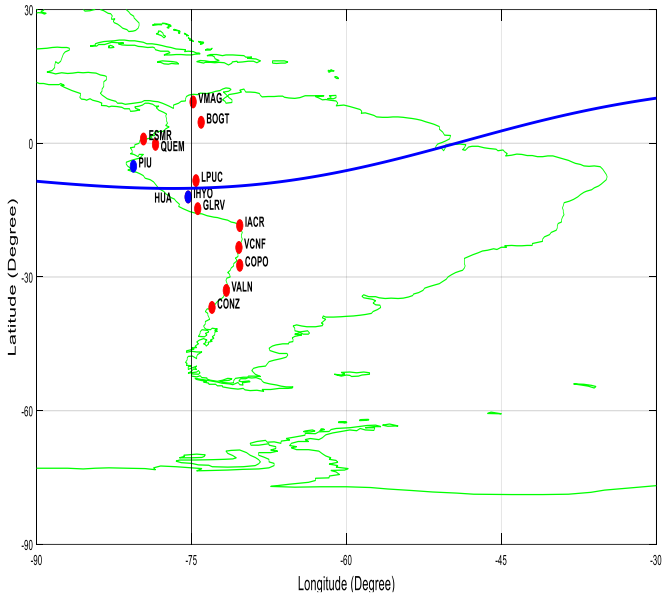

545

546 Figure1: A map showing the American low latitude GPS stations used in this investigation.

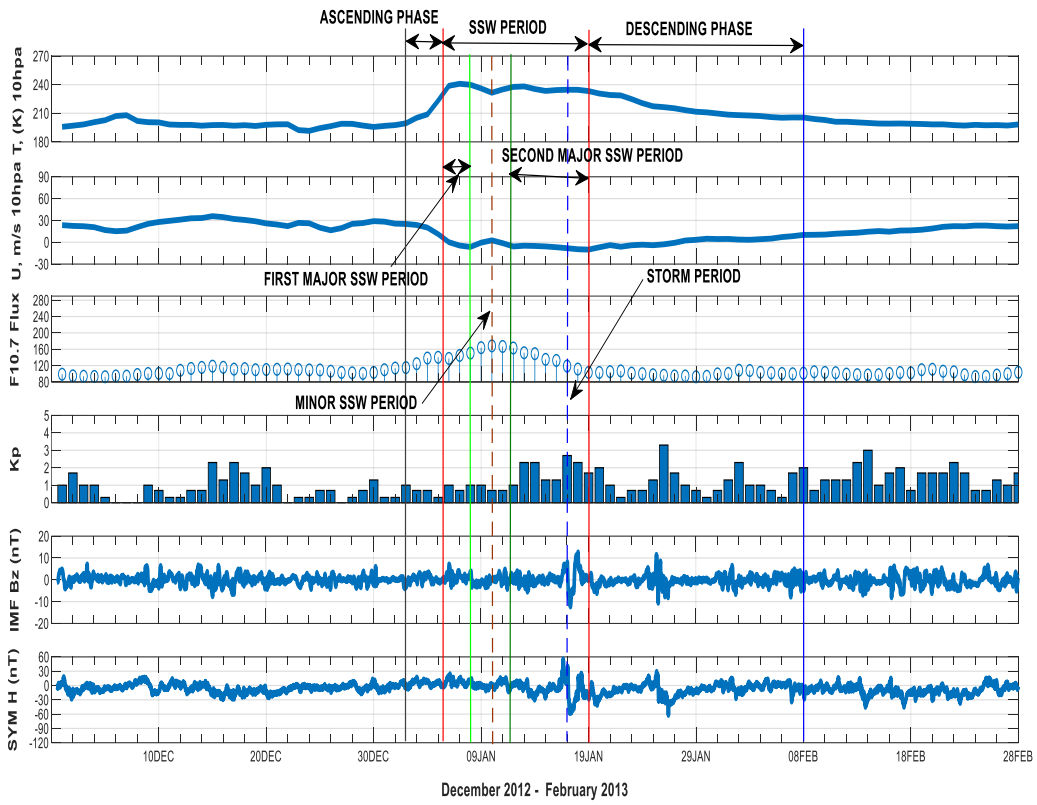

547

548 Figure 2: The stratospheric, solar, and geomagnetic parameters during December 2012 – February
549 2013 SSW events. The two vertical solid red lines and dashed blue line indicate the peak of the
550 SSW events and the period of minor the geomagnetic storm, respectively.

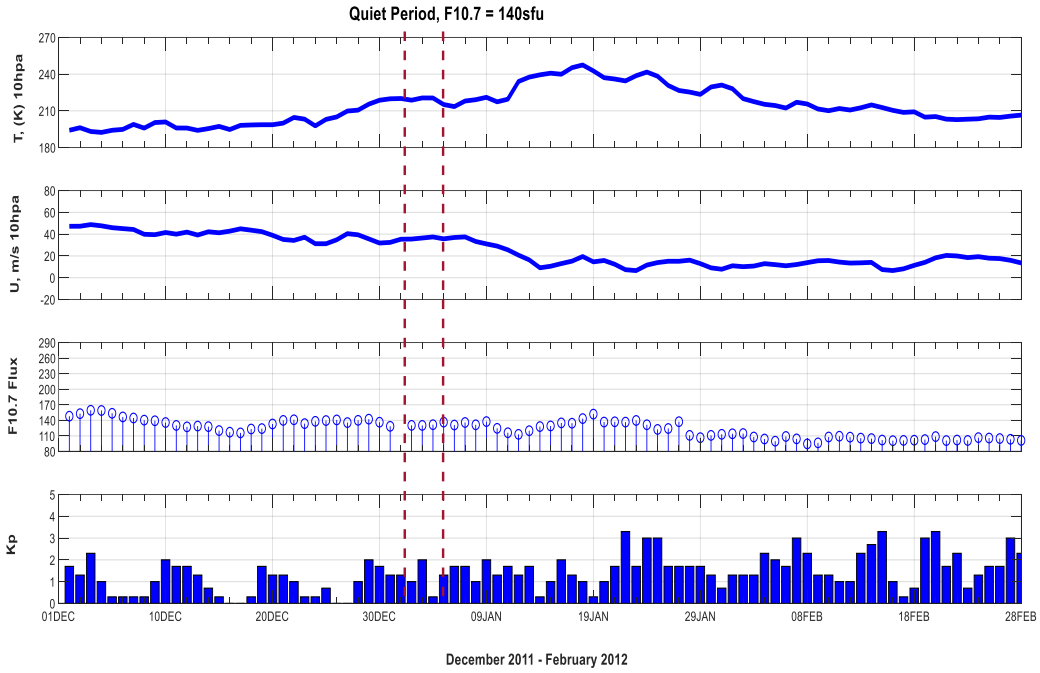

Figure 3: The stratospheric, solar, and geomagnetic parameters during December 2011 – February 2012 SSW events. The two vertical dashed brown lines indicate the period when solar flux, $F_{10.7}$ = 140 sfu (2-4 January 2012).

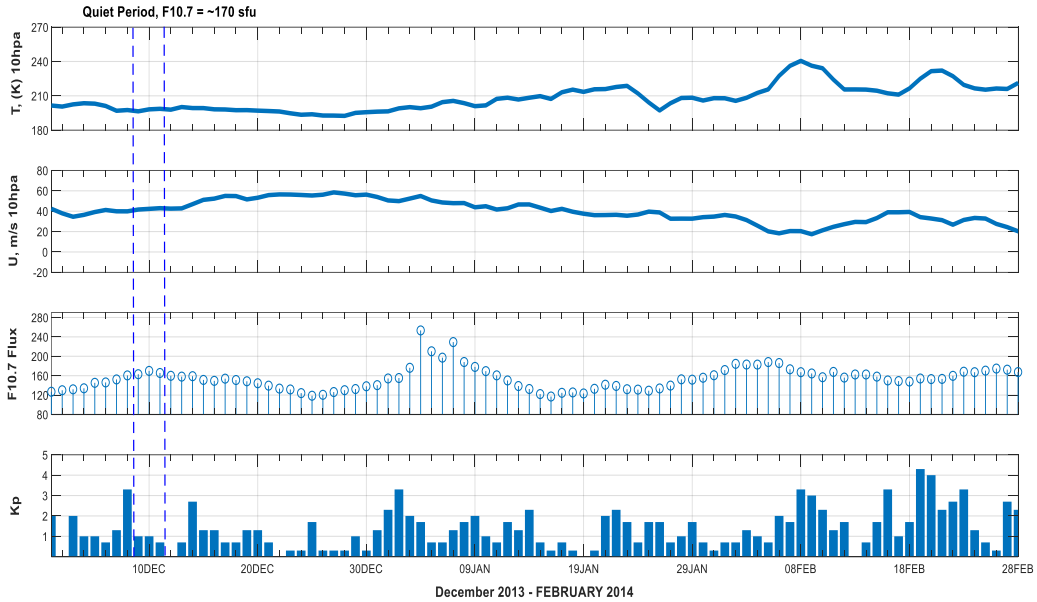

Figure 4: The stratospheric, solar, and geomagnetic parameters during December 2013 – February 2014 SSW events. The two vertical dashed blue lines indicate the period when the solar flux, $F_{10.7}$ = 168.2 sfu (9-11 December 2013).

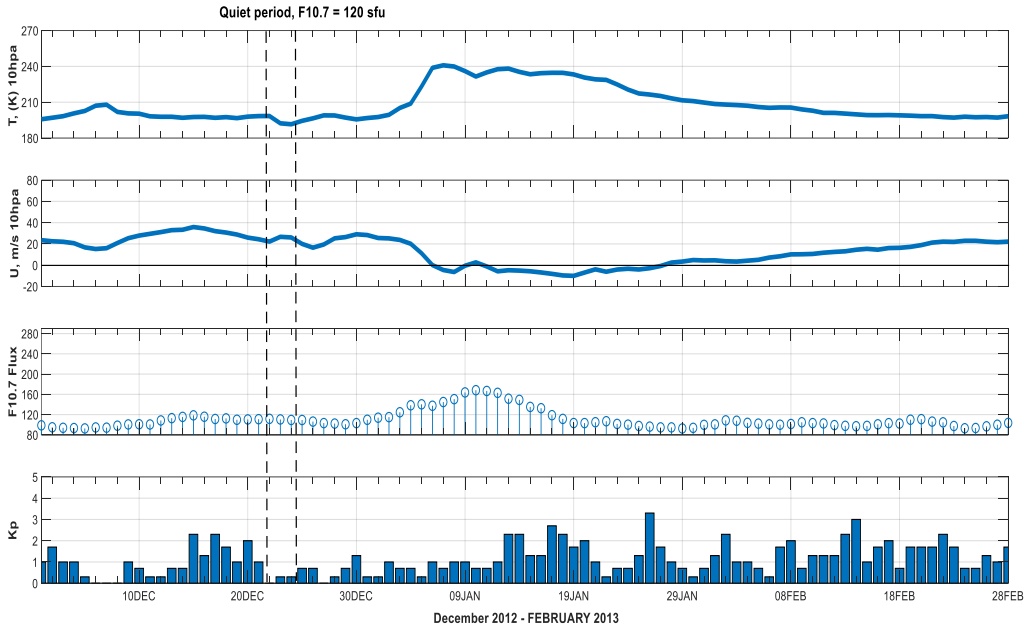

Figure 5: The stratospheric, solar, and geomagnetic parameters during December 2012 – February 2013 SSW events. The two vertical dashed black lines indicate the period when the solar flux, $F_{10.7}$ = 120 sfu (22-24 December 2012).

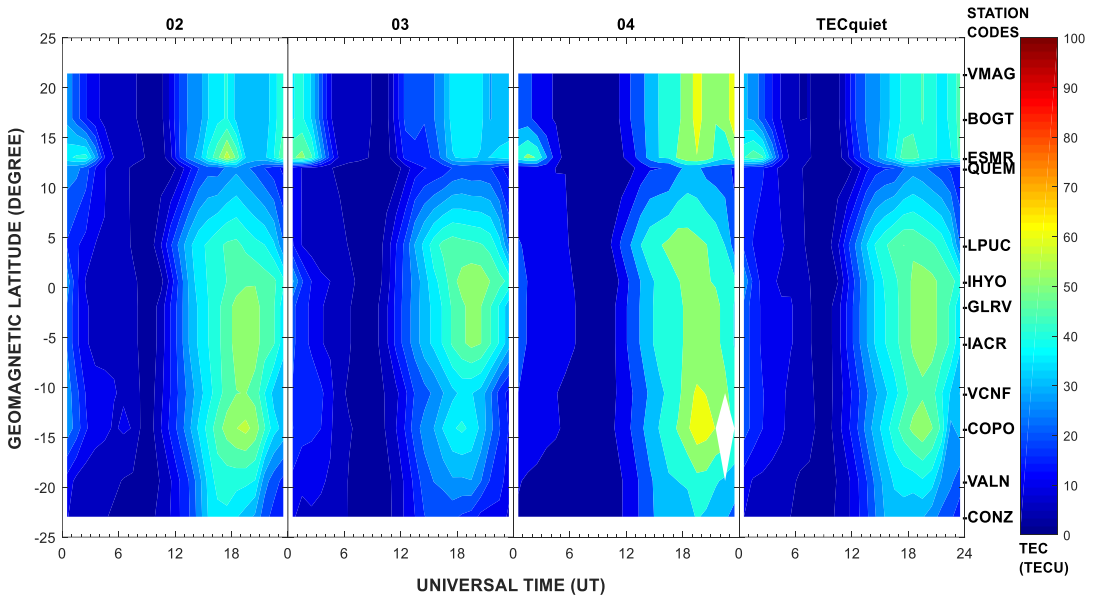

569

570 Figure 6: The daily TEC variations and averaged TEC value (TECquiet) during the periods when
571 the $F_{10.7}$ = 140 sfu (2 - 4 January, 2012) in the American sector.

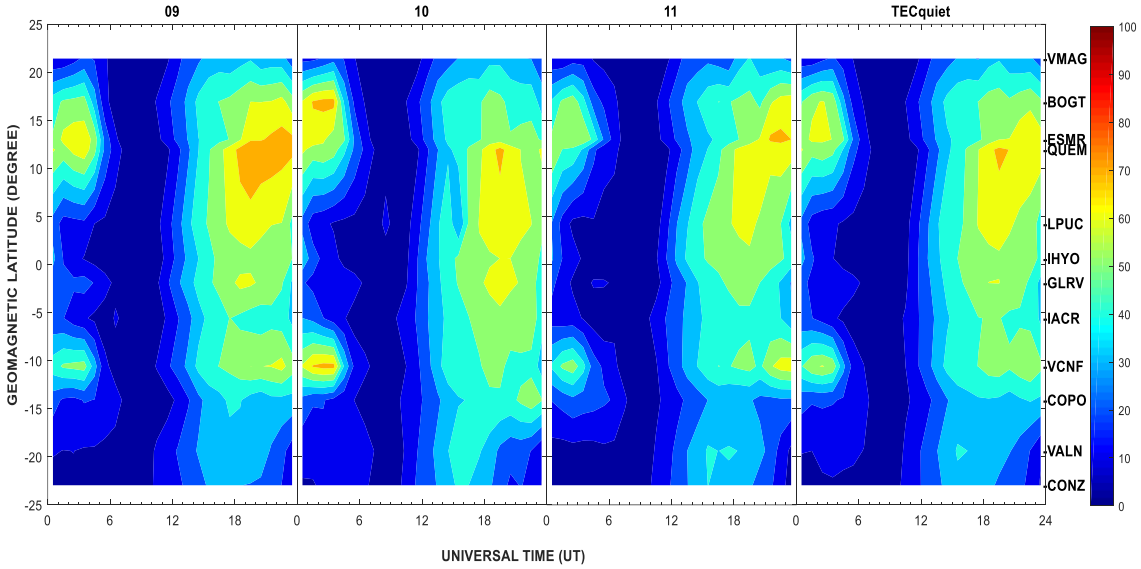

572

573 Figure 7: The daily TEC variations and averaged TEC value (TECquiet) during the periods when
574 the $F_{10.7}$ = 166.2 sfu (9 - 11 December, 2013) in the American sector.

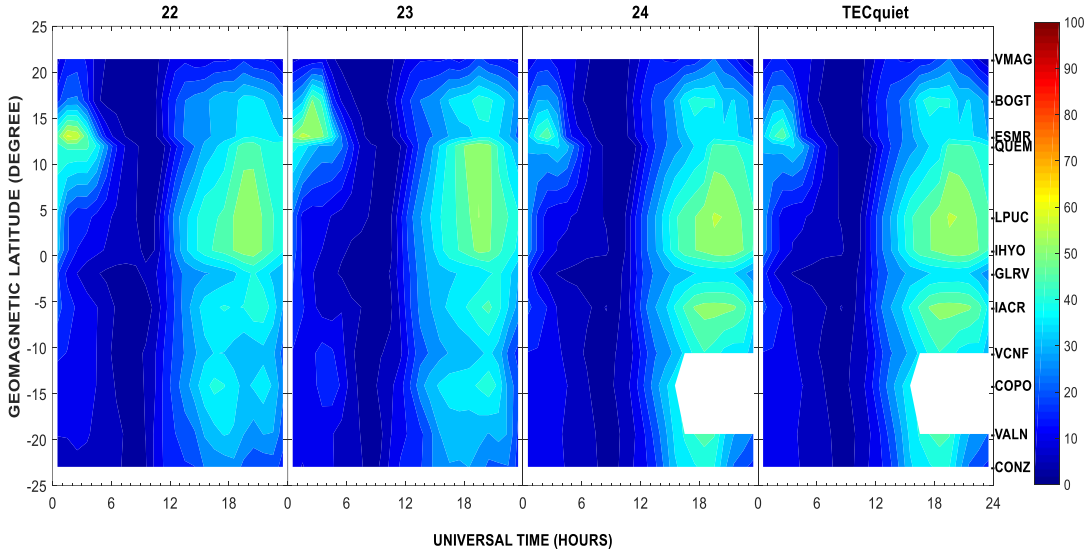

Figure 8: The daily TEC variations and averaged TEC value (TECquiet) during the periods when the $F_{10.7}$ = 120 sfu (22 - 24 December, 2012) in the American sector.

Table 2: Showing the individual contribution of F10.7, SSW, and geomagnetic storm during the Major and Minor warmings.

07/01/2013	F10.7 (%)	SSW Contribution (%)	Storm Contribution (%)
Northern Hemisphere	84	16	NIL
Southern Hemisphere	85	15	NIL
10/01/2013			
Northern Hemisphere	90	10	NIL
Southern Hemisphere	77	23	NIL
15-16/01/2013			
Northern Hemisphere	42	58	NIL

Southern Hemisphere	72	28	NIL
17/01/2013			
Northern Hemisphere	51	50	-1
Southern Hemisphere	58	20	22

581

582

583

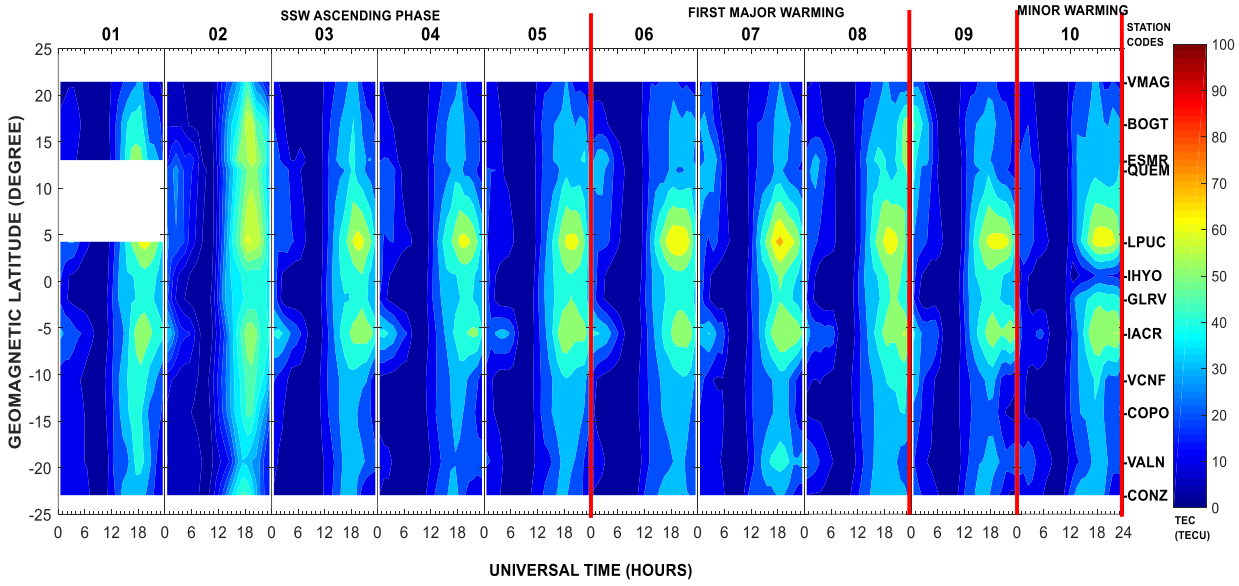

584

585 Figure 9a: The day-to-day variability of the American EIA from 01-10 January 2013.

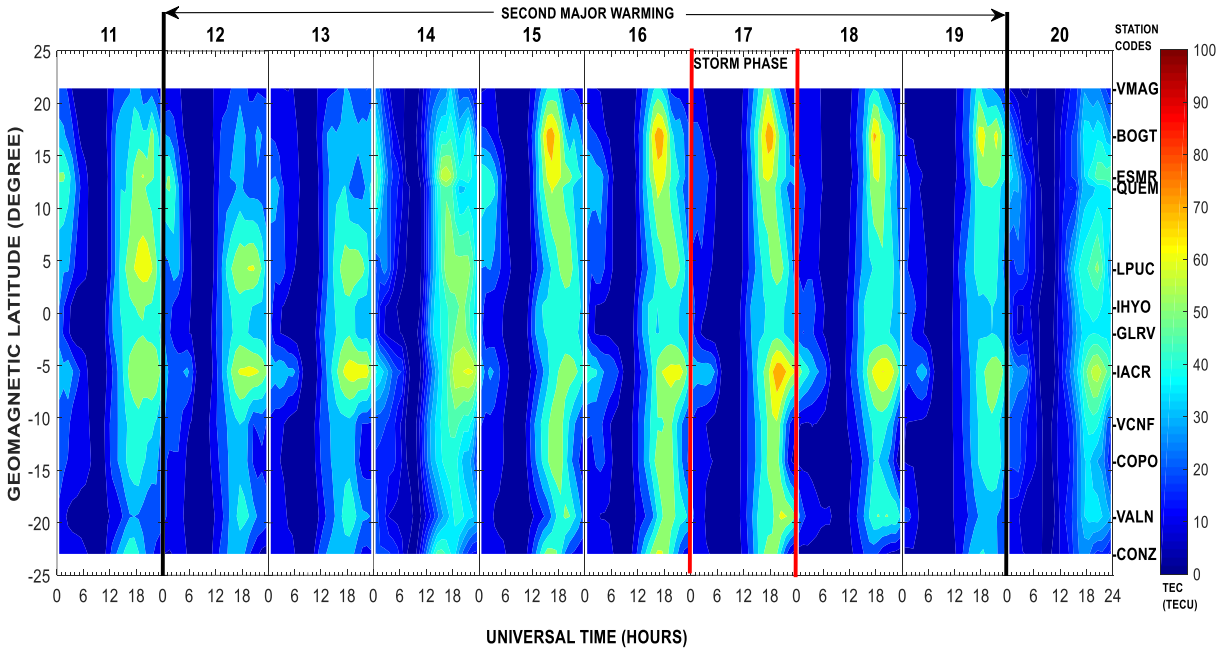

586

587 Figure 9b: The day-to-day variability of the American EIA from 11-20 January 2013.

588 **(a)**

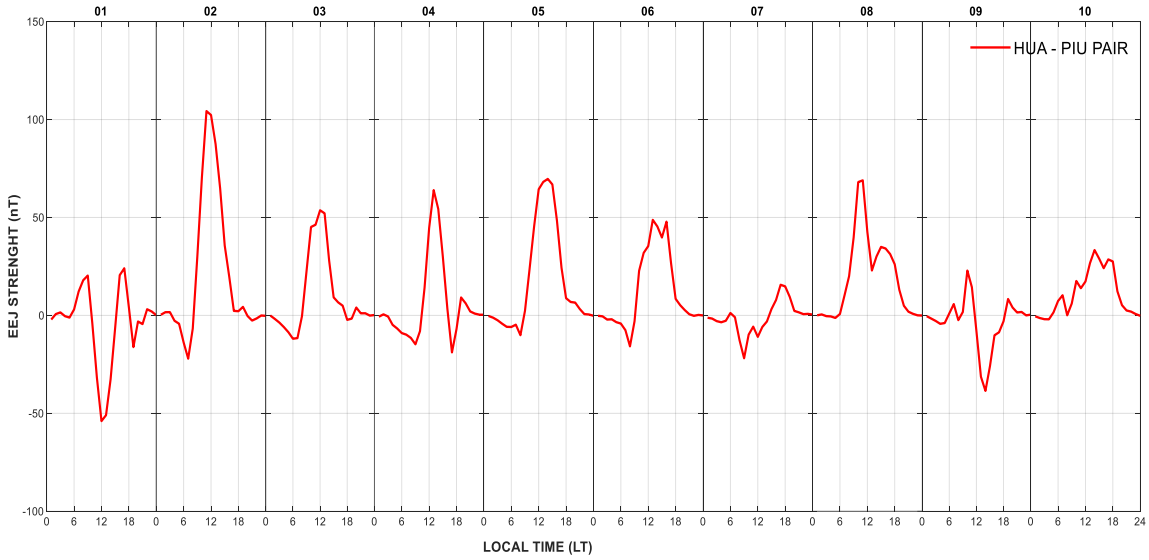

589

590 **(b)**

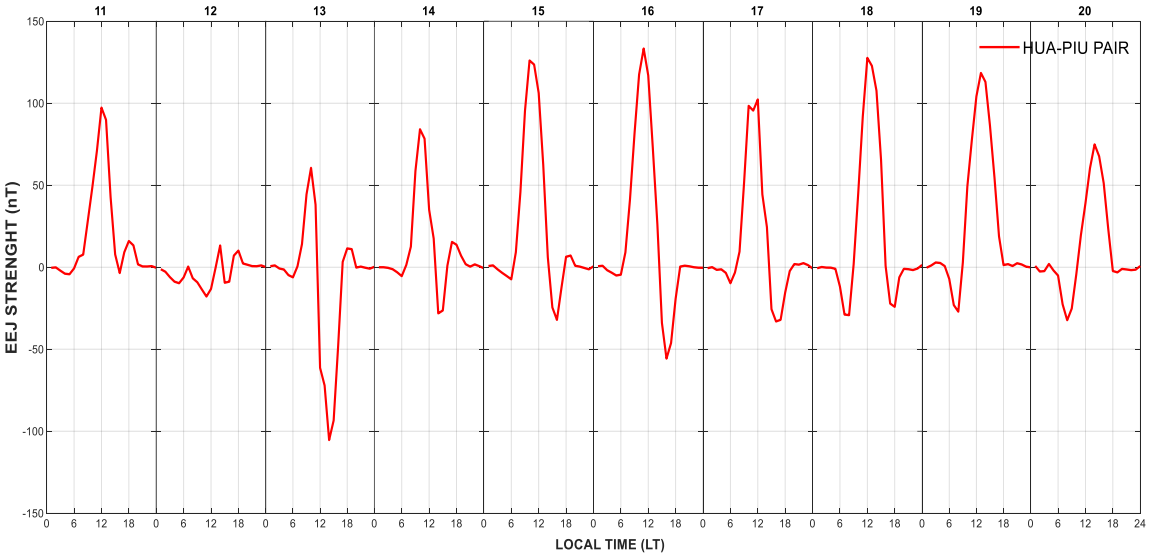

591

592 Figure 14 a and b: The inferred E X B drift over the Northern Hemisphere in the South America

593 during January 2013 SSW events.

594

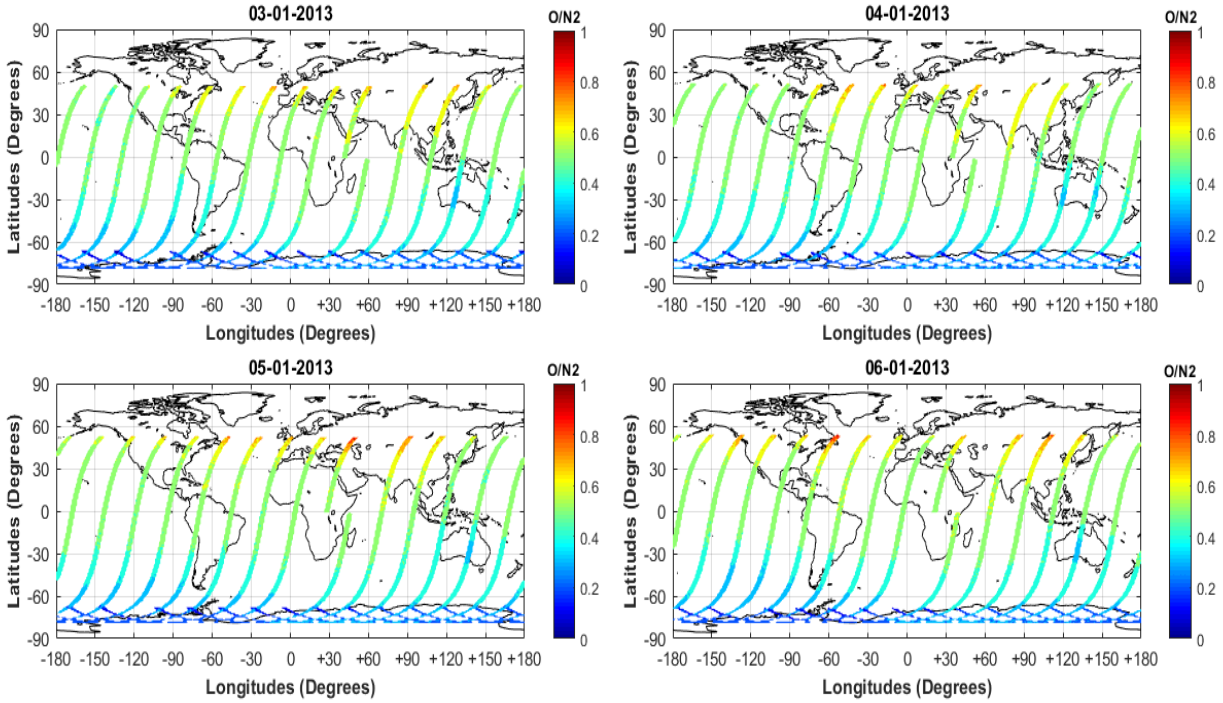

595

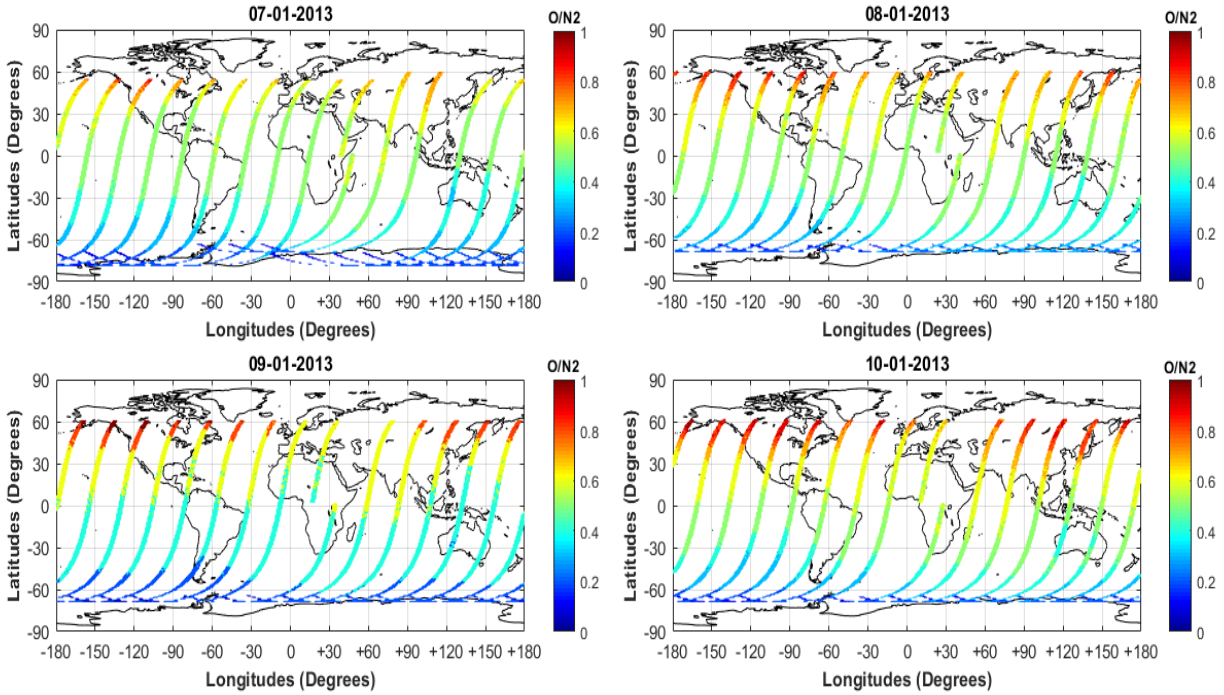
07-01-2013
08-01-2013
09-01-2013
10-01-2013
O/N2
Latitudes (Degrees)
Longitudes (Degrees)
90 60 30 0 -30 -60 -90
-180 -150 -120 -90 -60 -30 0 +30 +60 +90 +120 +150 +180
1 0.8 0.6 0.4 0.2 0

596

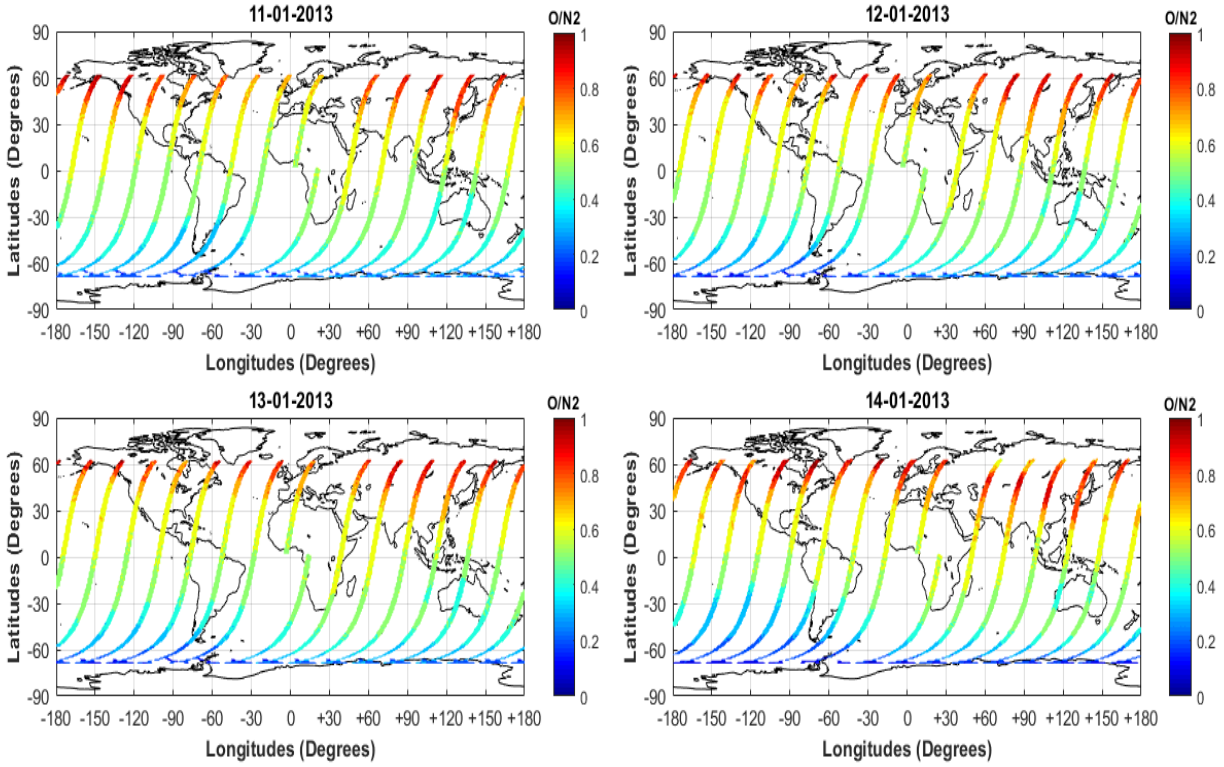
11-01-2013
12-01-2013
13-01-2013
14-01-2013
O/N2
Latitudes (Degrees)
Longitudes (Degrees)
90 60 30 0 -30 -60 -90
-180 -150 -120 -90 -60 -30 0 +30 +60 +90 +120 +150 +180
1 0.8 0.6 0.4 0.2 0

597

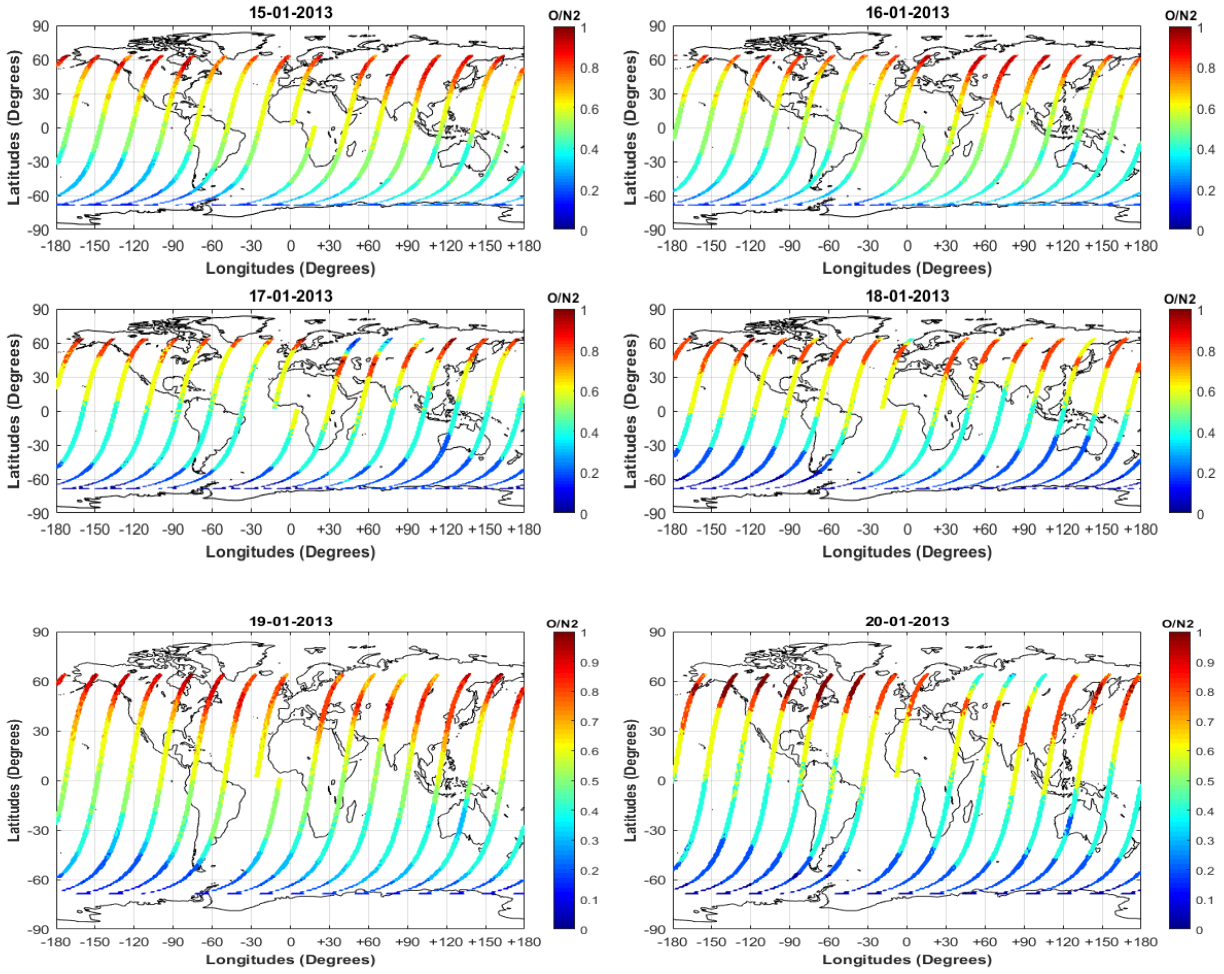

Figure 15: Thermospheric O/N_2 ratio from GUVI for the period of 03 – 20 January 2013.